Part 1 The study of some problems in near field optics

Chapter 4

The imaging properties of 3D aperture NSOM and optimized near-field fiber probes designs

Yuan-Fong Chau , Tzong-Jer Yang and Din Pin Tsai

A paper was deemed acceptable by the Japanese Journal of Applied Physics Part 1, Regular paper, 2004/04/08

4.1 Introduction

The major problem in near field scanning optical microscopes (NSOM) [1,2,3,4] is the determination of field distributions and radiation properties of a given probe/sample structure. Therefore, the precise spatial resolution depends upon such factors as the taper angle, the diameter of tip opening, refractive index of inner dielectric material of the coated probes, thickness and shape of the metal coating, and polarization and mode pattern of the excitation, all of which can affect the field pattern near the tip. In addition, the presence of the object being scanned can interact with the near field pattern, depending upon the electromagnetic properties of the object, causing it to change from its unobstructed behavior. A better understanding will lead to an unambiguous analysis of an NSOM image and will make the NSOM the more reliable imaging tool for both biologically interesting samples and nanostructured materials. Due to the complicated boundary conditions imposed by numerical methods only, requiring extended computational work. Experimental limitations in general prevent the direct probing of near fields. So far, the questions of achievable resolution and contrast have been left mainly to heuristic arguments and experimental evidence. It also requires for correct interpretation of NSOM images, by no means trivial task as will be seen from the results to be presented here. In the past, several efficient methods were implemented to overcome the difficulties raised by the complex geometry of such optical systems. Memory requirement is important in particular for calculating the three dimensionally distributed field with probe and sample. It has been done by means of using the dipole approximation method (DAM)[5], the boundary element method (BEM)[6], the multiple multi-pole method (MMP)[7, 8], the finite element method (FEM)[9], the Green tensors method[10, 11], and the FDTD method[12,13,14]. Among these methods, the FDTD method reduces the computer memory amount for the same 3-D model than the others, and solves Maxwell's equations

without any simplifying approximately other than the discretized grid, the method is well suited to simulate near field configurations and has been proved to be fruitful for solving near field optical problems[15,16,17,18,19,20,21]. Since the resolution provided by the 2 D model NSOM is lower than expected on the basis of experiments and can not handle a complex probe-sample system. Of the several possible reasons, the soft decay of the fields in 2 D ($r^{(-1/2)}$ instead of $r^{(-1)}$) might be the most fundamental one. This shows the need for 3D calculations which, however, require much longer computation times. Because of treating metals as a perfect conductor [22,23,24] cause concern that the optics in the near field region surrounded by metal may not be simulated accurately.

In this chapter, the treatment of dispersive metals in a time domain dependent fashion is considered. Little has been known if and how the emerging light from the tip lose the characteristics of polarization, after exiting from the tip apex, produces two perpendicularity polarized electric field components. This phenomenon of near field effeect will be described here. In this chapter, we investigate from a three-dimensional model, different aspects of this local interaction. Firstly, we will discuss some preliminary results recorded with the near field distribution of subwavelength circular aperture in an infinite aluminum plane to construct the foundation of latter analysis. The following section will compare the field distributions produced by two kinds of tips (non-coated and metal-coated) and give a suggestion for fabricating an optimal tip.

4.2 Numerical method

The finite difference time domain method is a flexible numerical means of solving electromagnetic problems by integrating Maxwell's differential equations,

$$\nabla \times H = \varepsilon(r)\frac{\partial E}{\partial t} + \sigma(r)E$$

$$\nabla \times E = -\mu(r)\frac{\partial E}{\partial t} \qquad \textbf{(4.1)}$$

for an arbitrary geometry in three-dimensional space. Where ε (r), μ(r), σ (r) are the position dependent permittivity, permeability, and conductivity of the material, respectively. The vectorial wave equation, issued from these equations, must then be solved in the specific

conditions imposed by the nature and the geometry of the tip-sample junction. When the surfaces limiting the illuminated objects display a complicated shape simultaneously with strong variations of the dielectric functions, seeking solutions of these universal equation needs specific care. We employed the numerical technique known as Finite-difference time domain (FDTD) for this analysis. The FDTD method treats Maxwell equation as a set of Finite difference equations in both time and space. The model space considered includes both the probe and the sample surface and consists of an aggregation of cubic cells with each cell which divides the model to be analyzed into a gridwork of small square or cuboidal cells, called "Yee cells" with each cell are positioned vector components of the electric field and magnetic field for the cell location. This object definition mechanism is the heart of the flexibility of FDTD, as any arbitrary geometry can be simulated. Each cell is assigned the susceptibility for a given material. The FDTD method calculates the electric and magnetic fields in each cell by integrating the Maxwell's equations in a "leap-frog" fashion until the steady state is reached [14]. In the case of the Gaussian pulse modulate with a sinusoidal excitation source, the steady state is reached (that is, the fields are not changing in peak-to-peak amplitude) when all scattered fields vary sinusoidally in time. The size of each cell is limited on the upper bound to be no longer than about one-tenth of the wavelength in order to assure sufficient sampling of the spatially varying fields. However, near field problems are well within this length limitation, and in fact there is no lower limit on the size of the Yee cell in terms of wavelength. Such small cells result in extremely short time steps in thesimulation, as the FDTD algorithm is stable only if

$$\Delta t \le \frac{1}{c\sqrt{\Delta x^{-2} + \Delta y^{-2} + \Delta z^{-2}}} \qquad \textbf{(4.2)}$$

where c is speed of light, $\triangle$ is the side of a cubical cell. This is a result of the Courant stability condition, which has its basis in the fact that the plane wave traveling in the FDTD space must not travel through more one cell in space of a time. The Finite difference equations corresponding to Ampere's law based on central difference approximation resulting in an explicit time-stepping algorithm, the Finite-difference form of this equation for the z-component of electric field in any given Yee cell can be written as:

$$E_z^{n+1}\left(i,j,k+\frac{1}{2}\right)=\frac{1-\dfrac{\sigma(i,j,k)\cdot\Delta t}{2\varepsilon(i,j,k)}}{1+\dfrac{\sigma(i,j,k)\cdot\Delta t}{2\varepsilon(i,j,k)}}E_z^n\left(i,j,k+\frac{1}{2}\right)+\frac{\dfrac{\Delta t}{\varepsilon(i,j,k)\cdot\Delta}}{1+\dfrac{\sigma(i,j,k)\cdot\Delta t}{2\varepsilon(i,j,k)}}\cdot$$
$$\left\{H_y^{n-\frac{1}{2}}\left(i+\frac{1}{2},j,k+\frac{1}{2}\right)-H_y^{n-\frac{1}{2}}\left(i-\frac{1}{2},j,k+\frac{1}{2}\right)+H_x^{n-\frac{1}{2}}\left(i,j-\frac{1}{2},k+\frac{1}{2}\right)-H_x^{n-\frac{1}{2}}\left(i,j+\frac{1}{2},k+\frac{1}{2}\right)\right\}$$

(4.3)

The magnetic induction elements H_x are calculated using Farad's law of induction:

$$H_z^{n+1/2}(i+\frac{1}{2},j+\frac{1}{2},k)=H_z^{n-1/2}(i+\frac{1}{2},j+\frac{1}{2},k)-\frac{\Delta t}{\mu(i+\frac{1}{2},j+\frac{1}{2},k)\cdot\Delta}\cdot$$
$$\left\{E_y^n(i+1,j+\frac{1}{2},k)-E_y^n(i,j+\frac{1}{2},k)+E_x^n(i+\frac{1}{2},j,k)-E_x^n(i+\frac{1}{2},j+1,k)\right\}\quad(4.4)$$

The updating equations for x- and y-components are obtained by rotation of in-dices, where the subscript on each field value gives its polarization and cell location. $\Delta x=\Delta y=\Delta z=\Delta$ are the lengths of the cell in the three directions, respectively, Δ is the unit time increment, and the superscript n is for time stepping, the refractive index is related to the permittivity $\varepsilon^{1/2}$, ($i\Delta x, j\Delta y, k\Delta z$) is a grid pint, ε (i, *j*, *k*) is the permittivity at ($i\Delta x, j\Delta y, k\Delta z$) , and similarly electrical conductivity σ (i, *j*. *k*) and permeability μ(i,j,k). Special consideration should be given at the boundary of the finite computational domain, where the fields are updated using special boundary conditions as information out of the domain is not available. The outside of the simulation area is considered to be the boundary of perfectly matched layer (PML) absorption [25], so that the electromagnetic field arriving at the boundary is not reflect but is perfectly absorbed by PML. Hence one can obtain the electromagnetic field inside the calculated space.

Typically, FDTD calculations have been carried out for dielectric materials. For noble metals (aluminum, gold, silver, and copper) in the optical regime posses complex refractive indices in which the imaginary part is greater than the real component. At optical frequencies the permittivity which is defined in the frequency domain is complex, with the real part of the permittivity being negative [26, 27]. In the case of inserting a negative real permittivity in the FDTD algorithms will cause the unstable situations in simulating process. This cause the apparent sign change in $D(\omega)$ (the Fourier transform of electric displacement). The sign change is caused by a material response that is 180^0 out of phase with respect to the electric

incident on the medium. To represent real metals correctly and maintain numerical stability require that a second order materials model for the medium be included in the FDTD scheme. Values for the complex refractive index for many materials including the noble metals have been measured and tabulated in the *CRC* laser handbook [28]. Refer to [29], the materials with frequency dependent, complex dielectric constants have been developed for treating dispersive materials in a time dependent form. The relation among electric displacement *D*, dielectric constant ε , and electric field *E* are

$$D(r,t) = \int_0^t \varepsilon(r,\tau)E(r,t-\tau)d\tau \tag{4.5}$$

We used the recursive convolution scheme(RC) method to evaluate the system which includes a dispersive medium such as metal films[30]. The relative dielectric constant in frequency domain is

$$\varepsilon_r(\omega) = \varepsilon_\infty + \chi(w) \tag{4.6}$$

where ε_∞ is the infinite frequency permittivity, χ is the susceptibility, ω is the angular frequency. If $\chi(\infty)= 0$, then the Eq.(5) can be expressed as

$$D(t) = \varepsilon_0\varepsilon_\infty E(t) + \int_0^t \chi(\tau)E(t-\tau)d\tau \tag{4.7}$$

Here, $\chi(\tau)$ is the Fourier transform of $\chi(\omega)$, and ε_0 is the permittivity of free space. The frequency domain Lorentz dispersion model can be designed to give the correct refractive index for any material at a single ω.

The refractive index associated with the Lorentz model, $n_L(\omega)$, has the form

$$n_L^2(\omega) = \varepsilon_R(\omega) = \frac{\chi_0\omega_0^2}{\omega_0^2 - \omega^2 + j\Gamma\omega} + \frac{\varepsilon_\infty}{\varepsilon_0} \tag{4.8}$$

where ε_R, ω_0 and Γ are the total complex permittivity, the resonant frequency and the damping coefficient for the model, respectively. The relations between ε_R and n_r (the

real part of the refractive index) and n_i (the imaginary part of the refractive index) can be expressed as

$$\varepsilon_R(\omega) = (n_L(w))^2 = (n_r^2 - n_i^2) + 2jn_r n_i$$

$$\varepsilon(\omega) = 1 + \frac{\omega_p^2}{\omega(iv_c - \omega)} = \varepsilon_\infty + \chi(\omega) \qquad \textbf{(4.9)}$$

where ω_p is the radian plasma frequency, and v_c is the collision angular frequency. The Drude model reveals the simple physical picture of a free electron gas [31]. The response of near field probes has been simulated under the Drude model using FDTD with some success [21]. We note that this Lorentz dispersion model contains the standard Drude model for metals as a limiting case. One obtains the Drude model by taking limit $\omega >> \omega_0$ and introducing the plasma frequency $\omega_p^2 = \chi_0 \omega_0^2$ and the collision frequency $v_c = \Gamma/2\pi$. For calculating the permittivity of the materials, one can choose reasonable DC and high-frequency response χ_0 and ε_∞ then solves for ω_0 and Γ and can be given by

$$w_0^2 = \frac{\omega^2}{1 - \chi_0(\varepsilon_r - \varepsilon_\infty/\varepsilon_0)/[(\varepsilon_r - \varepsilon_\infty/\varepsilon_0)^2 + \varepsilon_i^2]} \qquad \textbf{(4.10)}$$

$$\Gamma = \frac{\omega\chi_0\varepsilon_i}{(\varepsilon_r - \varepsilon_\infty/\varepsilon_0)^2 + \varepsilon_i^2 - \chi_0(\varepsilon_r - \varepsilon_\infty/\varepsilon_0)} \qquad \textbf{(4.11)}$$

The parameters are adjusted to closely match the experimentally observed optical properties. We set χ_0=10 and ε_∞=2.98 ε_0 in this work. The refractive indices for metal materials (Aluminum) in our simulations at wavelength λ =488 nm (ω=3.86×$10^{15}$$s^{-1}$) is -34.5 + *i*8.5[32]. From the Eqs. (10) and (11) the values for ω_0 and Γ are obtained for the material and the time domain version of the Lorentz model with these parameters is included in the FDTD computation in the metal ¯lm region of the numerical mesh.

4.3 The models and results

4.3.1 Subwavelength circular aperture image when the sample interactions are included

The optical properties for the metals have been of interest for more than 100 years.[35] During the past century, there are many important literatures concerned about it, such as the form of the solution to the problem of light scattering by spherical metal particle.[36] Other high-symmetry forms, including finite thickness slabs, cylinders, and ellipsoids, have been analytically solved.[37] The analytical solutions require only the particle size and frequency-dependent index of refraction $n = n_r + i\, n_i$, with the real part, n_r, representing the index of refraction, and the imaginary part, n_i, representing the extinction coefficient. In the real near-field optical recording systems, the light can be expressed as a wave vector and consists of only a real component in the normal state. The wave vector has a scale value $2\pi n/\lambda$, where n and λ mean the refractive index and wavelength, respectively. In metal, the component of the wave vector will be larger than the above scalar value when it is dispersed from the situation of high frequency or total internal reflection from the interface between two different materials. The component of the wave vector becomes purely imaginary, and thus this wave cannot be a propagation wave but an evanescent wave in one spatial direction, resulting in an exponential decay within a small distance compared to its wavelength. Since the optical properties in near field zone are much different compared to the far field zone. However, we can obtain the high quality resolution beyond the diffraction limit of an optical wave if we used the evanescent wave within the very short distance from the interface. The resolution of the evanescent wave has no relationship to its wavelength and reaches below 100 nm and has already been applied in the area of NSOM.[38] Although the thin metal plate with a subwavelength circular aperture with a sample interactions is a simple case, we think it is important to the near field region and necessary to make more detail analysis for the foundation of our latter simulations. The two sets of equations described by Eqs. (4.3) and (4.4) are alternately evaluated to simulate the light propagation. In the past decade, there were two different setups have been developed from this basic configuration: (1)The transmission illumination mode in which the light radiated by a nanometric emitter is converted into propagating waves by the sample itself. (2) The transmission collection mode which is easily obtained by reversing the light path. The aperture plays the role of a nano-collector, and the light converted in the near-field zone is transmitted to a photo-detector. We will discuss the transmission collection mode in this section. Figure 1, shows a schematic diagram of the 3-D subwavelength circular aperture with a sample model to be analyzed. It has an aperture opening of 80 nm (40 cells) in an infinite aluminum thin metal plate with the thickness of 40 nm (20 cells), a dielectric sample with the refractive index of n=1.5, and the distance between the aperture and the sample surface is 20 nm (10 cells), filled with silica core inside the

aperture and the bottom of the model as shown in Fig. 1. The surface profile of dielectric sample consists of a flat surface with single cylindrical protrusion whose height and diameter are 20 nm (10 cells), 120nm (60cells), respectively. Another difficulty in the FDTD method is the error caused by the incident light on the incident surface. Total field/scattered field formulation13) is used to introduce the incident light into the calculation space. The frequency of the source is $4.74 \times 10^{14} Hz$, corresponding to a free-space wavelength of 633 nm, which propagates from base plane to the aperture, located at the plane shown in Fig.1. The dimensions of each cell are $\Delta x = \Delta y = \Delta z = 2$nm, and the total space volume considered measures $100(x) \times 100(y) \times 100(z)$ cells.

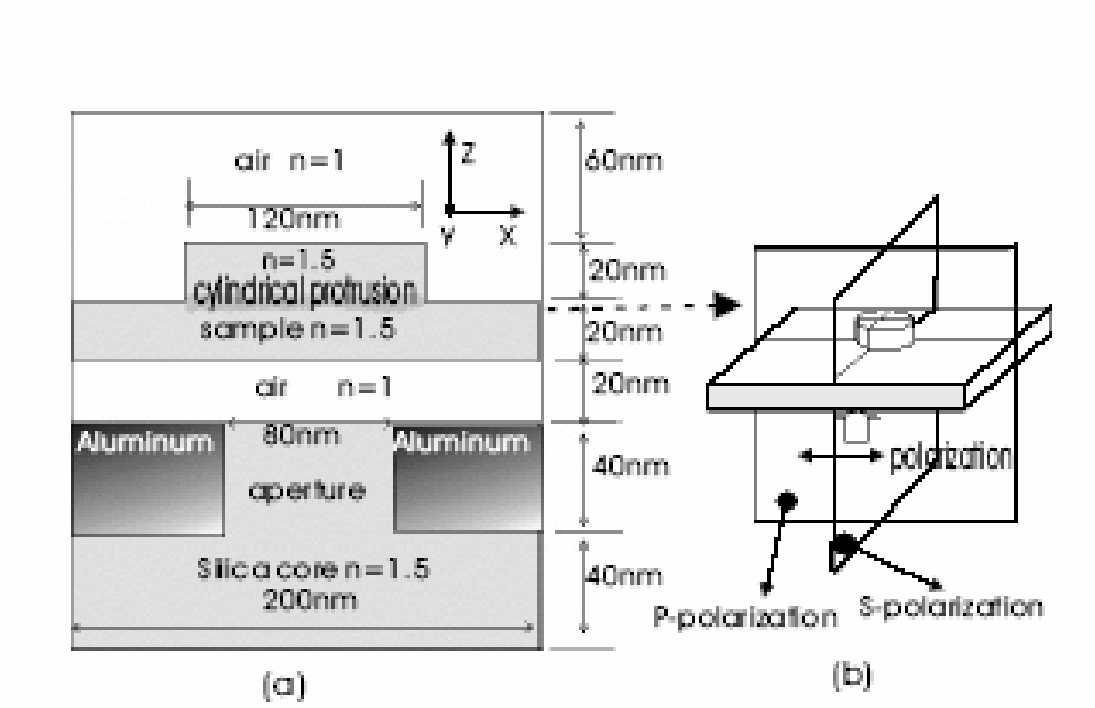

Fig. 4.1 Geometry of three-dimensional subwavelength circular aperture with sample interaction. (a) Sectional plane diagram of 3-D subwavelength circular aperture when the sample interactions are included. (b) Convention used when considering the effects of two orthogonal polarization states (s polarization and p polarization). The incident electric field is p-polarized when the electric field vector oscillates in a sectional plane that is perpendicular to the surface of the edge structure. On the other hand, s-polarization occurs when the field oscillates in normal direction to a sectional plane.

The effects of light polarization on the generated near-field images are studied for both parallel and perpendicular polarization conditions. When the model structure possess a preferred orientation, the characteristics of the scattered light depend on the polarization direction (either parallel or perpendicular) relative to the structure orientation. In this paper, we define that the incident electric field is p-polarized when the electric field vector oscillates

in a sectional plane that is perpendicular to the surface of the edge structure. On the other hand, s-polarization occurs when the field oscillates in normal direction to a sectional plane. Figs. 2(a)-(d) show the calculated results of the three-dimensional electric field for p-polarization and s-polarization illumination, respectively. In the gray-scale used, white is used to signify higher intensity values. Although this model is a rotational symmetric system, the electric field distributions formed in the two orthogonal cross sections are different from each other due to the difference between the boundary conditions in edge interface. This result implies that the resolution of an aperture NSOM is given by the size of the aperture rim, which is a great advantage of an aperture NSOM. In a NSOM with an aperture in metal coating,[15] the penetration of photons through the metal coating smears the spot, so that the practical minimum size of the spot is at least practically 50 nm in diameter even if an extremely small aperture is used. In the sectional image of the model illuminated by p-polarization shown in Fig.2(a) and (b), the intensity becomes stronger near the edges of aperture and sample, and the image generated agree reasonably with the geometrical profile of the same model shown in Fig.1. The field enhancement is due to the surface plasmon

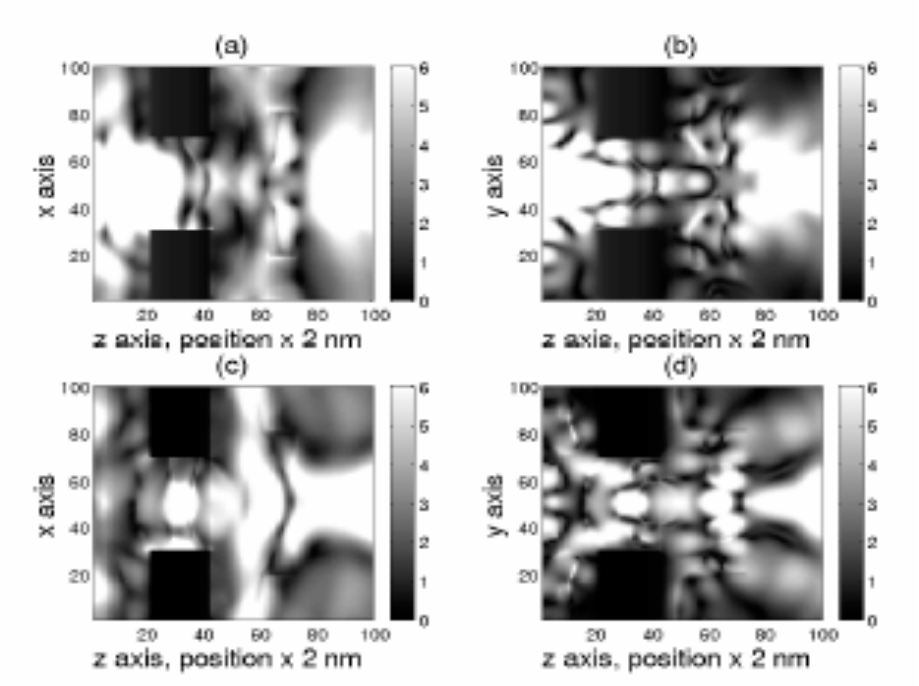

Fig. 4.2 Distribution of the 3-D electric field intensity modulus around the aperture-sample coupling zone: (a) in x-z plane (at y=50△), p-polarization, (b) in y-z plane (at x=50 △), p-polarization, (c) in x-z plane (at y=50△), s-polarization, and (d) in y-z plane (at x=50△), s-polarization, respectively. The electric field results from an incident wave coming from the left side. In the gray-scale used, white is used to signify higher intensity values.